Chemical Engineering Journal 149 (2009) 428–434

Contents lists available at ScienceDirect

Chemical Engineering Journal

journal homepage: www.elsevier.com/locate/cej

Hydrodynamic focusing studies in microreactors using voltammetric analysis: Theory and experiment

Abhishek G. Deshpande[a], Yungfen Gu[a], Sinéad M. Matthews[a], Kamran Yunus[a], Nigel K.H. Slater[a,*], Colin M. Brennan[b], Adrian C. Fisher[a]

[a] Department of Chemical Engineering, University of Cambridge, New Museums Site, Pembroke Street, Cambridge CB2 3RA, UK
[b] Syngenta Ltd., Huddersfield Manufacturing Centre, PO Box A38, Leeds Road, Huddersfield HD2 1FF, UK

ARTICLE INFO

Article history:
Received 7 July 2008
Received in revised form 26 January 2009
Accepted 31 January 2009

Keywords:
Microfluidics
Voltammetry
Microfabrication
Hydrodynamic focusing

ABSTRACT

The article describes a numerical and experimental investigation of the voltammetric response observed within small-scale electrochemical reactors, where reagents are directed to a sensor electrode using hydrodynamic focusing. A microelectrochemical reactor was developed, fabricated and tested for electrochemical sensitivity. The studies presented examine the influence of stream velocity, lead-in length and focusing stream ratios on the electrolytic current induced. The numerical models reveal a regime where the finely focused stream of reagent responds in an identical manner to a cell completely full of reagent and also to a regime where diffusional broadening of the reagent stream into the carrier stream becomes significant with a resulting loss in voltammetric sensitivity. In addition at higher focusing ratios, where the reagent occupies a much smaller portion of the channel, full electrochemical depletion of the species is possible at substantially greater throughput rates than is feasible without the focusing arrangement. Experimental studies show qualitative agreement with numerical predictions.

1. Introduction and background

Hydrodynamic voltammetry is a well understood and established technique. It has been widely used in continuous chemical monitoring, high throughput screening and the mechanistic analysis of electrolysis processes [1–3]. Hydrodynamic voltammetry in microfluidic systems can be conducted by placing a working electrode smoothly into the wall of a rectangular duct and passing electrolyte solution through the cell under laminar flow conditions. Well defined mass transport conditions can be obtained by careful design of the channels, enabling analysis of the current/transport rate response of a specific system. Other microfluidic devices have found applications in chromatographic separations [4,5], spectroelectrochemical studies such as IR, UV/visible, ESR and fluorescence spectroscopy [6–10] and more recently we have demonstrated the voltammetric analysis in immiscible multiphase processes [11–13].

The development and application of microfluidic devices incorporating electrochemical sensors has expanded rapidly over recent years, although qualitative and quantitative current/voltage relationships with flow rate remain less well explored [14–16]. The ability to manipulate fluids at micro- and nano-litre scales offers significant potential for these combined microreactor/electrochemical devices in the fields of analysis and electrosynthesis [17].

One potential limitation of the approach results from the necessity for reagent transport to and from the electrode surface and this can result in a low percentage of the electroactive reagent being available at high throughput rates. One way of making a higher percentage of reagent available has been demonstrated by Horii et al. [17] in which a thin microchannel was employed with channel heights that were close to the diffusion layer thickness. More recently there has been considerable interest in hydrodynamic focusing, which seeks to confine a sample into a narrow stream (see Fig. 1) by the use of a second liquid stream which acts to drive the reagent stream closer to the electrode sensor. This reduces the total quantity of reagent employed, while retaining cell geometries which permit high throughput characteristics. Yoon et al. [18] demonstrated focusing of reagent streams close to an electrode using a buffer stream of same phase. In a further application Krüger et al. [19] injected suspended cells in a laminar flow stream and hydrodynamically focused a flow of single cells to pass under a beam of monochromatic light. Wolff et al. [20] have developed a chimney-like sheathing structure in a microchannel for focusing of the cell sample. Another novel method of focusing has been addressed by Fu et al. [21] where the focusing of particles and liquids into a narrow beam using high voltages was achieved.

* Corresponding author. Tel.: +44 1223 762953; fax: +44 1223 334796.
E-mail address: nkhs2@cam.ac.uk (N.K.H. Slater).

1385-8947/$ – see front matter © 2009 Elsevier B.V. All rights reserved.
doi:10.1016/j.cej.2009.01.051

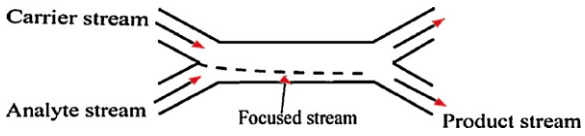

Fig. 1. Schematic of hydrodynamic focusing within a microfluidic device.

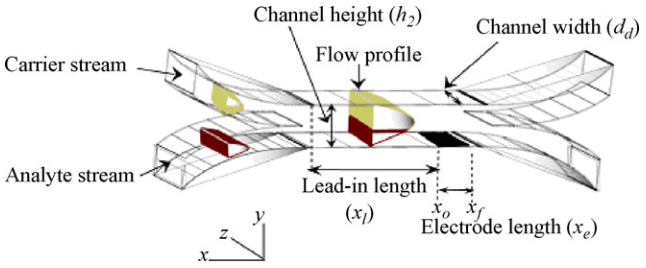

Fig. 2. Schematic of hydrodynamic focusing in a microchannel using 0.1 M KCl as background electrolyte and 1 mM potassium ferricyanide as the substrate stream.

Here, a numerical model is developed that describes the variation of current as a function of total volume flow rate (the combined flow rates of the analyte and carrier streams), lead-in length (distance between the point where two streams meet and the leading edge of the electrode) and focusing stream ratios (the ratio of carrier stream flow rate to analyte stream flow rate). The model is used to evaluate the effects of hydrodynamic focusing. An electrochemical cell in which two analyte streams were introduced was simulated using a finite difference model in order to determine the response of the device to hydrodynamic focusing. The results from the computational model were compared to those observed experimentally using microfabricated devices.

2. Theory

This article considers the transport limited reduction of species (A)

$$A + e^- \rightarrow B$$

at an electrode fabricated on one wall of a rectangular duct, a schematic of which is shown in Fig. 2.

It was assumed that sufficient electrolyte was present in solution to neglect transport effects induced by migration and that the diffusion coefficients of species A and B are matched. In this way we may either simulate reactant (A) or product (B) subject to application of appropriate boundary conditions at the inlet and electrode surface.

A finite difference scheme was adopted to simulate the coupled mass transfer and electrolysis reaction. A modified form of the backwards implicit (BI) scheme that we have reported previously for three-dimensional simulations with microreactors was employed [22]. A schematic of the mesh is shown in Fig. 3.

The relevant boundary conditions for an electrolysis reaction occurring at the electrode surface are:

$x_0 < x < x_f$	$y = 0$	$0 < z < d_d$	$[A] = 0$
$x_0 < x < x_f$	$y = 0$	$0 < z < d_d$	$i = Fx_e wD\left(\frac{\partial [A]}{\partial y}\right)_{y=0}$
$0 < x < x_0$	$y = 0$	$0 < z < d_d$	$\frac{\partial [A]}{\partial y} = 0$
$x_f < x$	$y = 0$	$0 < z < d_d$	$\frac{\partial [A]}{\partial y} = 0$
$0 < x$	$y = h_2$	$0 < z < d_d$	$\frac{\partial [A]}{\partial y} = 0$
$x > 0$	$0 < y < h_2$	$z = 0$	$\frac{\partial [A]}{\partial z} = 0$
$x > 0$	$0 < y < h_2$	$z = d_d$	$\frac{\partial [A]}{\partial z} = 0$

Where x_0 and x_f correspond to the start and end of the electrode in the x direction (see Fig. 3). The current was calculated using the following equation:

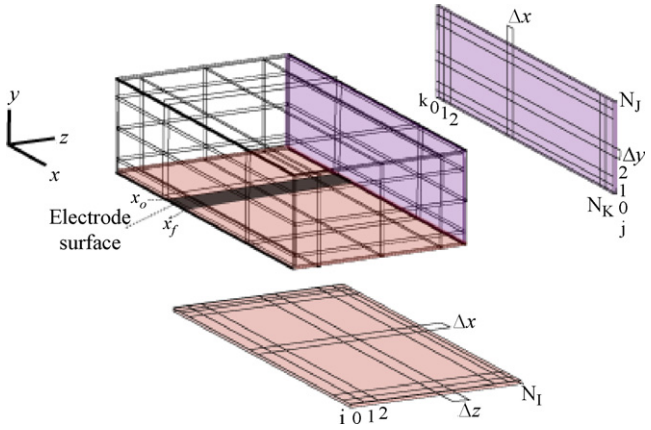

Fig. 3. Schematic of grid employed for numerical simulations.

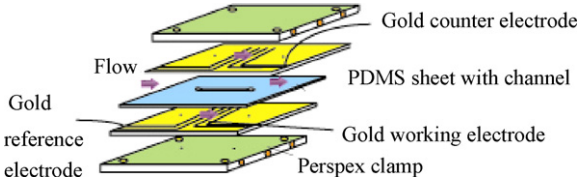

Fig. 4. Schematic of microelectrochemical reactor.

$$i = F D_A [A]_{bulk} \frac{\Delta x \, \Delta z}{\Delta y} \sum_{k=k_0}^{k=k_f} \sum_{i=1}^{i=N_I} ({}^t a_{i,l,k} - {}^t a_{i,0,k}) \quad (1)$$

where k_0 is the counters at the start of the electrode in the x direction, with k_f the corresponding box at the end of the electrode in the x direction.

3. Experimental

Microelectrochemical reactors were assembled by sandwiching a PDMS microgasket channel between two electrode plates (Fig. 4). The working and reference electrodes were fabricated on one of the glass substrates and the counter electrode on the other glass substrate, with a PDMS microchannel placed between them to define the channel sidewalls as illustrated in Fig. 4.

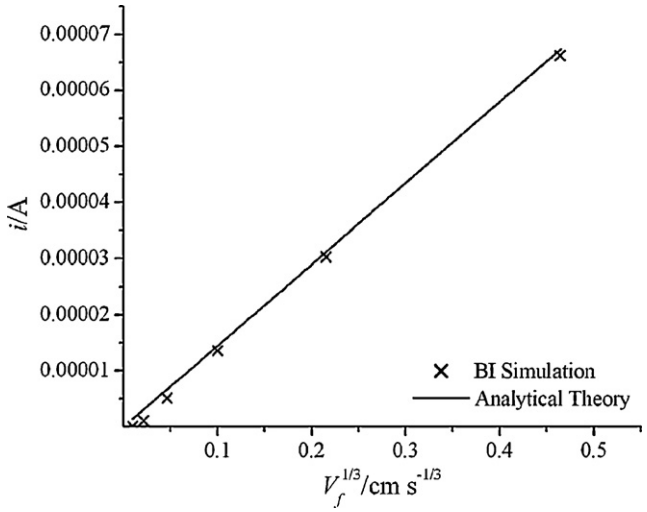

Fig. 5. Comparison of transport limited current predicted by BI and analytical simulation methods.

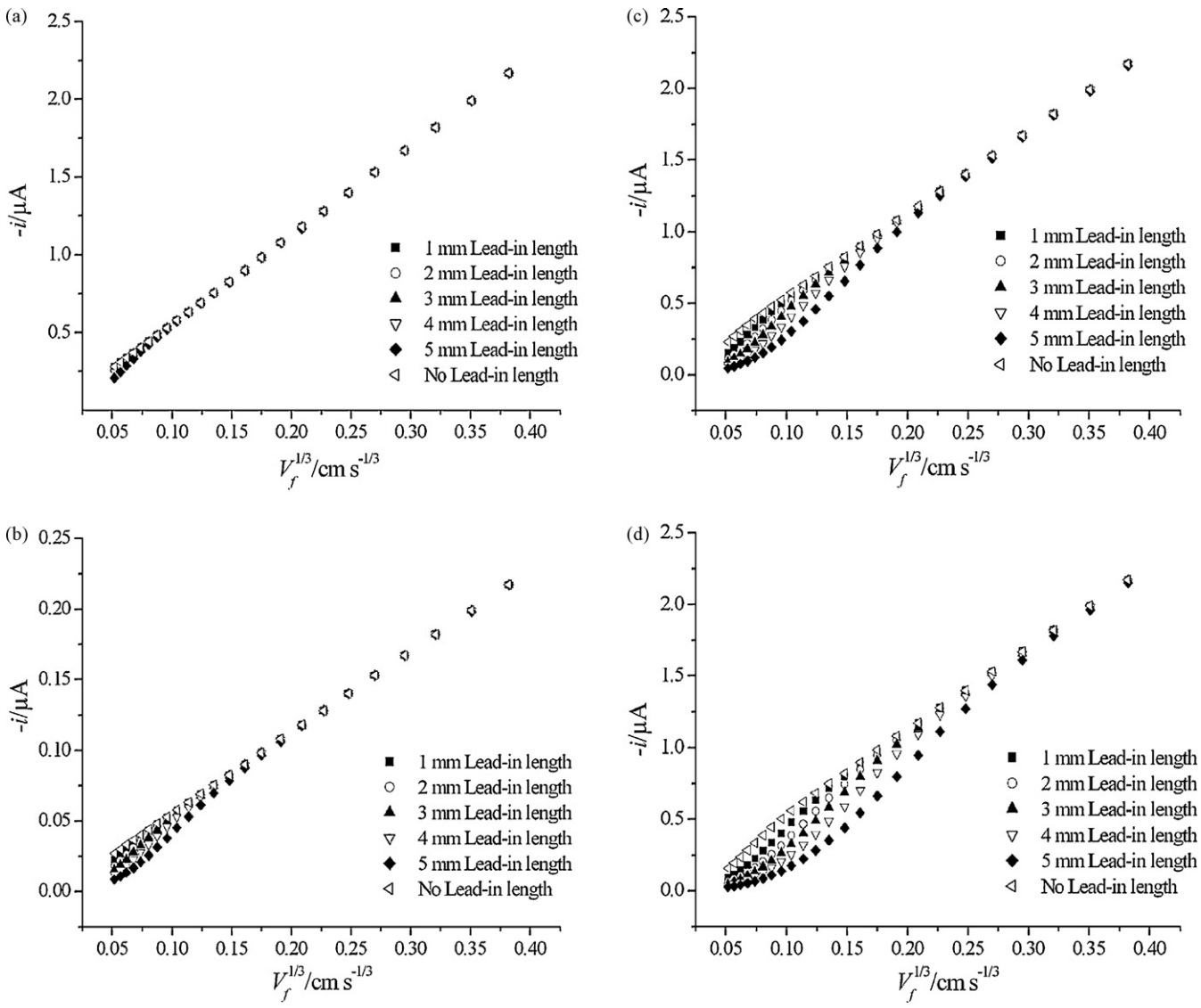

Fig. 6. Plots of steady state current against cube root of volume flow rate for focusing ratios of (a) 1:1, (b) 5:1, (c) 10:1 and (d) 20:1.

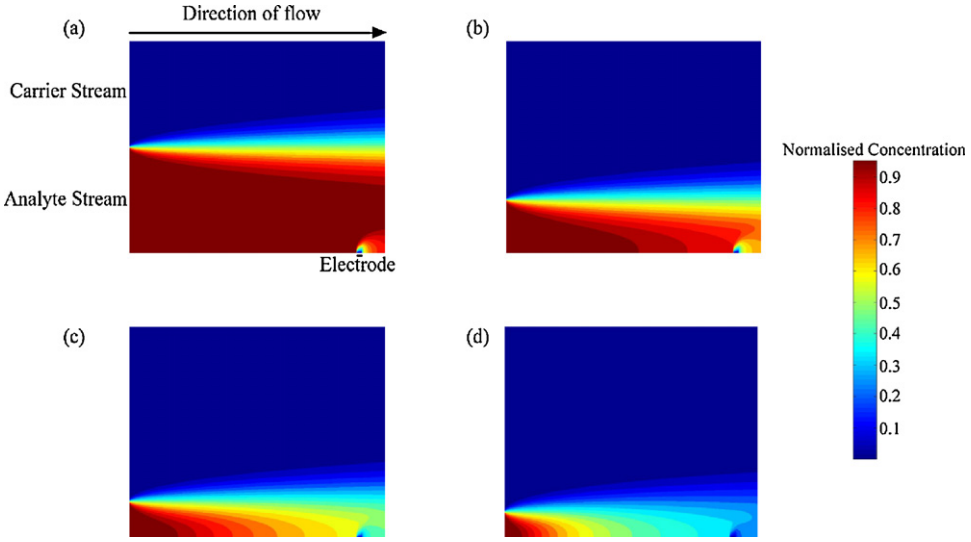

Fig. 7. Concentration profile taken along the centre of the cell for a lead-in length of 10 mm and focusing ratios of (a) 1:1, (b) 5:1, (c) 10:1 and (d) 20:1.

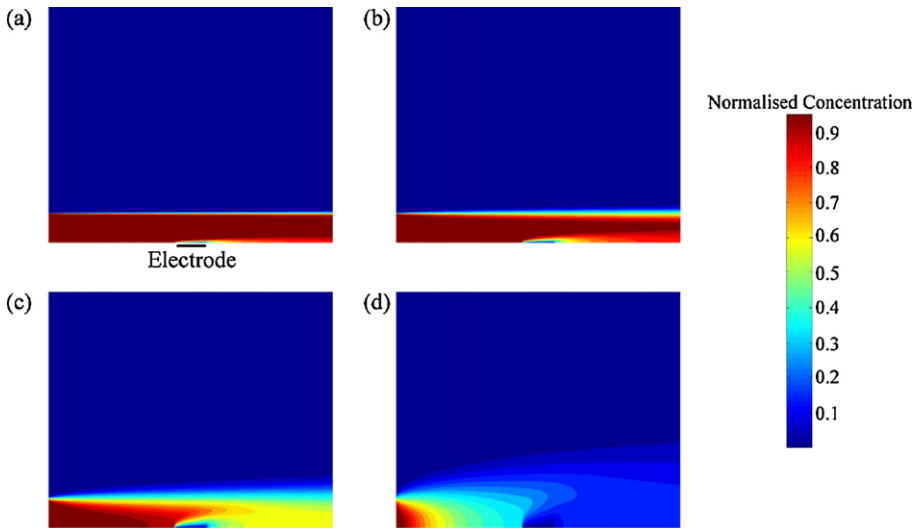

Fig. 8. Central concentration profiles for volume flow rates of (a) 7.5×10^{-2} cm^3 s^{-1}, (b) 1×10^{-2} cm^3 s^{-1}, (c) 1×10^{-3} cm^3 s^{-1} and (d) 1×10^{-4} cm^3 s^{-1} with a focusing ratio of 20:1.

The microfabrication procedure consisted of two stages, fabrication of gold microelectrodes and fabrication of a microchannel made from a PDMS microgasket.

3.1. Microelectrode fabrication

Glass wafers cut to size were treated with piranha solution (3:1 ratio of sulphuric acid to hydrogen peroxide) to clean the glass from any impurities. After treating the wafers for 5 min, the glass was rinsed thoroughly in milli-Q water before being blow dried with nitrogen. Using standard photolithographic techniques a desired electrode micropattern was created over the glass wafers with Microposit S1828 positive photoresist [23]. The patterned wafers were then coated with thin films of titanium and gold (approximately 20 and 150 nm respectively) using a metal evaporator (Edwards Auto 306). After the metal coating cycles, the wafers then underwent a lift off process to remove the photoresist mask leaving the desired gold microelectrode pattern coated over the glass wafers.

3.2. PDMS microgasket fabrication

Wafers were cleaned using the same approach as described above with piranha solution, and were used to create a micromould using SU8-2100 epoxy resin (Microchem) and standard photolithographic procedures [24]. These micromoulds were then spin coated with poly(dimethylsiloxane) (PDMS, Sylgard 184, Dow Corning) at 250 rpm for 1 min to obtain a film thickness of approximately 250 μm. The PDMS coated wafers were soft baked on a hot plate at 45 °C for 1 min and then cured in an oven at 60 °C for 2 h. After curing the PDMS, the SU8 photoresist was removed by immersing the wafers in 1,2-dichloroethane for 1 h to reveal the PDMS microgasket. The PDMS gasket was then sandwiched between the gold microelectrode wafers using a clamp system to create the microfluidic device.

Voltammetric measurements were carried out using a computer controlled PGSTAT 30 potentiostat (Autolab, Eco Chemie, Utrecht, The Netherlands). The fluid flow was controlled using two syringe pumps (Harvard Apparatus) with typical flow rates between 1.67×10^{-5} and 8.3×10^{-2} cm^3 s^{-1}.

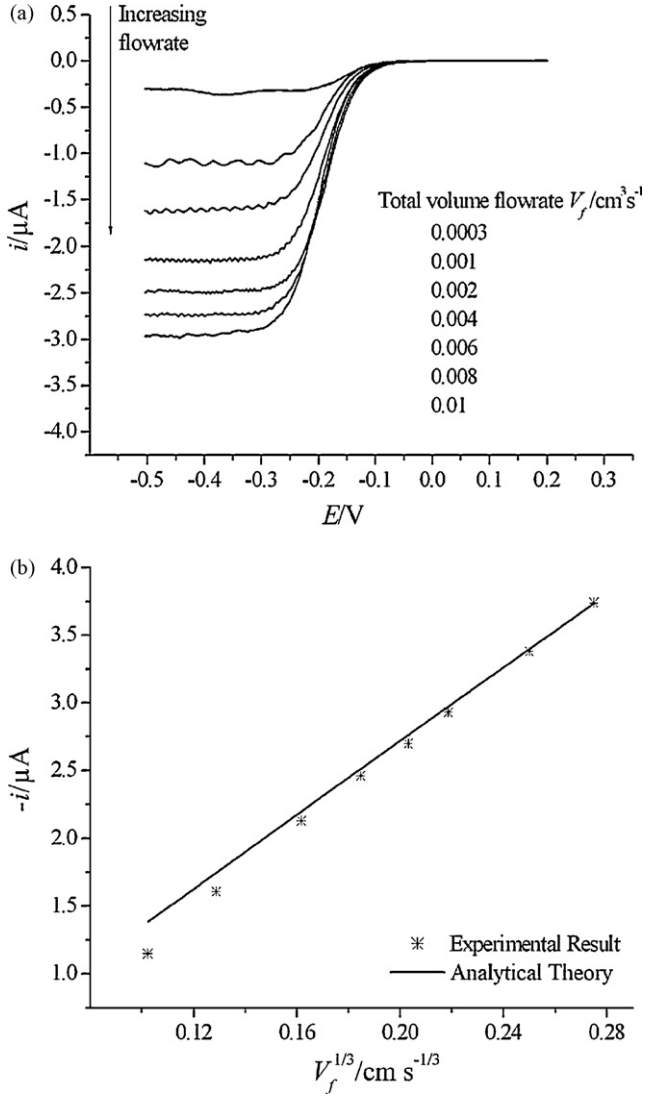

Fig. 9. (a) Sample voltammograms using 5:1 focusing ratio with a lead-in length of 2.1 mm and (b) limiting current against the cube root of the volume flow rate for the control experiment.

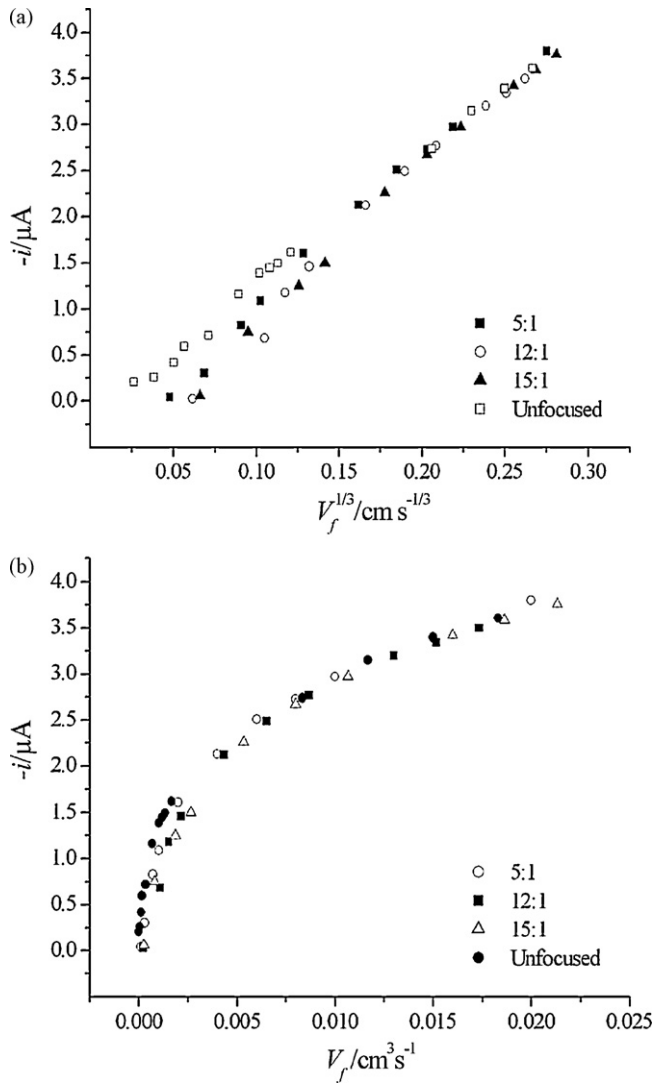

Fig. 10. Effect of focusing ratio (a) steady state current against cube root volume flow rate and (b) steady state current against volume flow rate.

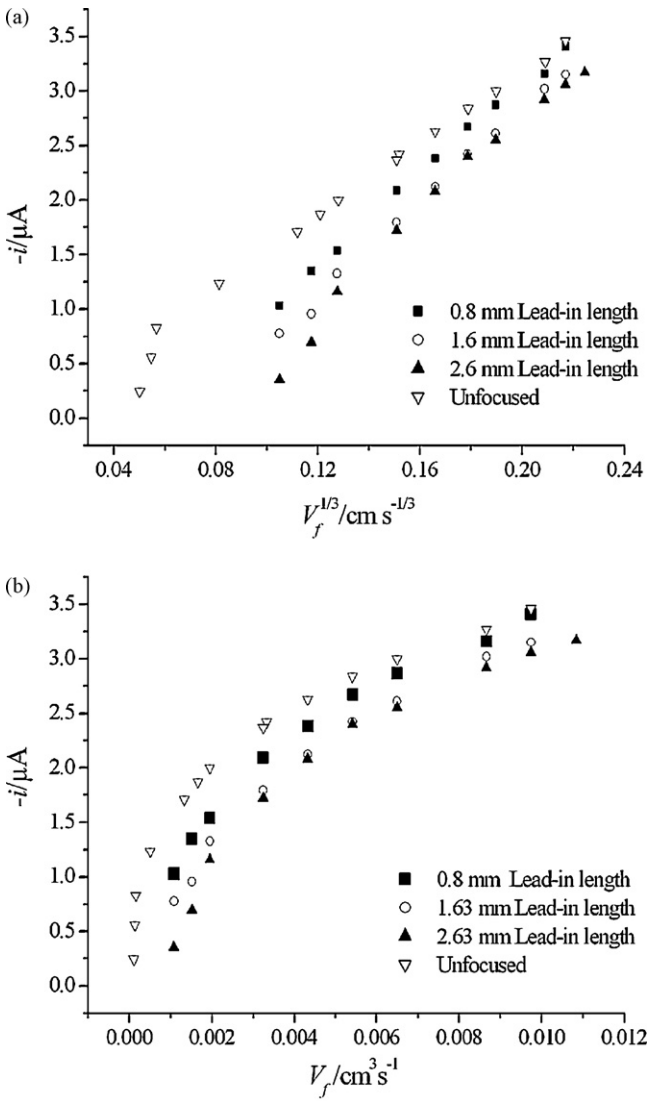

Fig. 11. Effect of lead-in length (a) steady state current against cube root volume flow rate and (b) steady state current against volume flow rate.

4. Results and discussion

4.1. Numerical simulations

In order to test the numerical codes, a cell in which both inlets supply a solution containing the bulk concentration of a species A was initially examined. In this case a 4 mm × 4 mm electrode was sited centrally within the bottom face of a duct of width 0.6 cm, height 0.04 cm. Under these conditions the hydrodynamic boundary layers at the edge of the channel are sufficiently small that they render the calculation analogous to a two-dimensional channel flow calculation and thus allow comparison of the voltammetric predictions with that expected from the Levich equation. Fig. 5 shows the predicted response for a microfluidic device employing the following parameters: $[A]_{bulk} = 10^{-6}$ mol cm^{-3}, $D_A = 10^{-5}$ cm^2 s^{-1}, $N_I = 20$, $N_K = 40$, $N_J = 200$, $V_f = 10^{-1}$–10^{-6} cm^3 s^{-1}.

Under these conditions it is established that axial convection and diffusion normal to the electrode surface are the dominant transport characteristics and therefore control the mass transport limited current. Also presented in Fig. 5 is the current predicted on the basis of the Levich equation. Agreement is observed between the two approaches.

Next the BI model was applied to the numerical investigation of variables affecting the performance of a microfluidic device with hydrodynamic focusing. As stated previously, three specific variables were examined: lead-in length, focusing ratio and total volume flow rate.

The effect of lead-in length on the current response was studied using 6 different lead-in lengths: 0, 1, 2, 3, 5 and 10 mm. Four different focusing ratios were simulated: 1:1, 5:1, 10:1 and 20:1 (see Fig. 6a–d) for each lead-in length. An electrode spanning the width of the channel was simulated using the following parameters: $h_2 = w_e = 0.05$ cm, $x_e = 0.025$ cm, $x_I = 0.0225$ cm, 0.325 cm, 0.425 cm, 0.525 cm, 0.725 cm and 1.225 cm (for lead-in lengths of 0, 1, 2, 3, 5 and 10 mm respectively), $N_J = 250$, $N_K = 2600$–9800, $N_I = 80$, $[A]_{bulk} = 10^{-6}$ mol cm^{-3}, $D_A = 10^{-5}$ cm^2 s^{-1} and $V_f = 0.0001$–0.05 cm^3 s^{-1}. Fig. 6a–d shows the datasets obtained for the different focusing ratios (1:1, 5:1, 10:1 and 20:1). At high volume flow rates the mass transport limited current for all cases converges to that expected for the whole cell filled with an electroactive agent. At lower flow rates the effect of lead-in length and transport rate show clear deviations resulting from diffusional broadening of the reagent into the carrier stream. Fig. 7a–d shows a series of concentration profiles taken from the central position

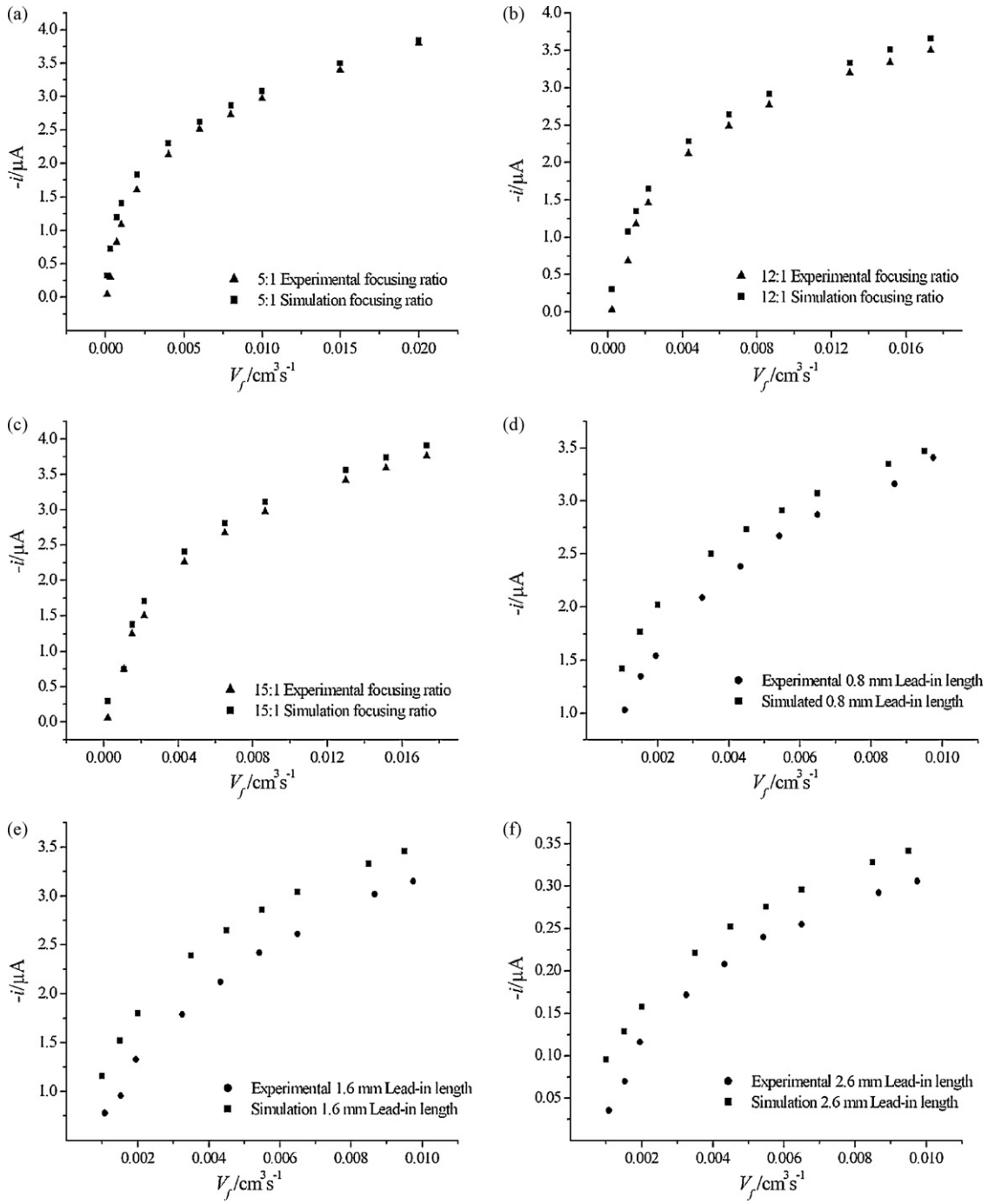

Fig. 12. Comparison of experimental and simulated steady state currents for focusing ratios of (a) 5:1, (b) 12:1, (c) 15:1 and comparison of experimental and simulated steady state currents for lead-in lengths of (d) 0.8 mm, (e) 1.6 mm, (f) 2.6 mm.

along the cell for a lead-in length of 10 mm at a total volume flow rate of 10^{-3} cm^3 s^{-1}. Fig. 8a–d shows the corresponding effects of volume flow rate from a focusing ratio of 20:1. Both sets of figures clearly demonstrate the effect of diffusional broadening on the reagent concentration within the device.

The numerical simulations illustrate the potential to employ hydrodynamic focusing as a method to reduce the quantity of reagent required within the device yet still obtain a response equivalent to a cell full of reagent, offering significant potential for cost and material savings in high throughput devices. In addition at higher focusing ratios the analyte stream occupies a much smaller portion of the channel enabling the electrochemical depletion of species A to extend to the full height of the analyte stream.

5. Experimental hydrodynamic focusing studies

Experimental studies were carried out to examine the effect of the three variables investigated using the numerical model: lead-in length, focusing ratio and total volume flow rate. An analyte stream containing 1×10^{-6} mol cm^{-3} potassium ferricyanide ($K_3Fe(CN)_6$) with 0.1×10^{-3} mol cm^{-3} potassium chloride and a carrier stream containing 0.1×10^{-3} mol cm^{-3} potassium chloride were employed for the focusing studies. In order to compare with standard channel electrode behaviour a control experiment where both streams contained potassium ferricyanide was also performed.

Flow to the device was controlled using two separate syringe pumps to regulate independently the flow rate of each stream.

Three different focusing ratios were studied—5:1, 12:1 and 15:1. The voltammetric response of potassium ferricyanide was measured using linear sweep voltammetry. The potential difference was scanned from 0.2 to −0.5 V (vs. gold pseudo-reference electrode) at a rate of 0.04 V s^{-1}. For each experiment voltammograms were recorded for a series of total volume flow rates between 1×10^{-2} and 1×10^{-4} cm^3 s^{-1}. Some sample voltammograms, obtained using a focusing ratio of 5:1 and a lead-in length of 2.1 mm, are shown in Fig. 9a. The channel was characterised using the unfocused control experiment where analyte was pumped through both inlets and the resulting variation of the transport limited current as a function of the cube root of volume flow rate is shown in Fig. 9b. The analytically predicted current is also shown and agreement between the two sets of data is observed.

Next focusing studies were carried out for the ratios 5:1, 12:1 and 15:1. Fig. 10 shows plots of the steady state current against both the cube root of the total volume flow rate and the total volume flow rate for each focusing ratio and the control (unfocused) experiment.

Fig. 10 illustrates that at higher flow rates, regardless of the focusing ratio, the current varies linearly with the cube root of the volume flow rate; indicating a standard voltammetric response. However, at low flow rates this linear relationship breaks down and the deviation from the expected response appears to be dependant on the focusing ratio. The lowest ratio (5:1) clearly deviates from the unfocused behaviour the least. The current response for the 12:1 and 15:1 are very similar and do overlap at some total volume flow rates, but in general the 15:1 focusing ratio deviates from the linear behaviour more than the 12:1 ratio.

Finally the effect of the lead-in length of the voltammetric response of the system was investigated using three different values: 0.8, 1.6 and 2.6 mm. A focusing ratio of 12:1 was used for all experiments. Fig. 11 shows the plots of steady state current against both volume flow rate and its cube root.

Fig. 11 shows that the current response varies linearly with the cube root of the volume flow rate. However, with increasing lead-in length the steady state current is reduced compared to the unfocused current. This effect is greatest at lower flow rates and longer lead-in lengths. These general trends are consistent with those predicted by the numerical model; as the lead-in length is increased more diffusive mixing between the streams can occur, reducing the flux of material to the electrode surface and as a result the current response is reduced.

Finally, the BI numerical model was used to simulate the experimental hydrodynamic focusing system. The parameters were: $h_2 = 0.025$ cm, $w_e = d_d = 0.089$, $x_e = 0.05$ cm, $x_l = 0.285$ cm, 0.365 cm and 0.465 cm (for 0.8 mm, 1.6 mm and 2.6 mm lead-in length respectively) $N_J = 500$, $N_K = 1000$–2000 (depending on the lead-in length), $N_l = 100$, $V_f = 0.0002$–0.02 cm^3 s^{-1}, $D = 6.77 \times 10^{-6}$ cm^2 s^{-1} and $[C] = 1 \times 10^{-6}$ mol cm^{-3}. Fig. 12a–e compares predicted and experimental responses. The model provides a qualitative description of the variation of current with volume flow rate, although absolute values of current are off-set by ∼0.5 μA. Though the trend of the plots was adequately described by the simulation, some off-set was seen at higher lead-in lengths. This off-set was due to experimental errors which were propagated and amplified with increasing lead-in length.

6. Conclusion

A microelectrochemical reactor based on a sandwich like structure was successfully developed, fabricated and employed for hydrodynamic focusing studies. Experimental studies examining the effects of focusing ratio, lead-in length and volume flow rate on the electrolysis response observed were carried out and compared to results predicted numerically using a finite difference model. Regimes where diffusional broadening of the reagent stream may affect the current response were identified. Diffusional broadening is low at high flow rates and hence electron transfer at the electrode occurs at the same rate as if the entire channel were filled with reactant. In contrast, diffusional broadening due to considerable lead-in lengths and high focusing ratios affect the concentration of reagents at the electrode surface at low flow rates resulting in slower electron transfer.

Acknowledgment

A.G.D. would like to thank Cambridge Commonwealth Trust and Bombay Cambridge Trust and S.M.M. would like to thank Syngenta Ltd. for funding and support.

References

[1] C.M.A. Brett, in: R.G. Compton, G. Hancock (Eds.), Comprehensive Chemical Kinetics, vol. 37, Elsevier, Amsterdam, 1999 (Chapter 16).
[2] C.M.A. Brett, A. Maria, Comp. Chem. Kinet. 26 (1986) 355.
[3] J.A. Cooper, R.G. Compton, Electroanalysis 10 (1998) 141.
[4] P.T. Kissinger, Anal. Chem. 477A (1997) 49.
[5] R.M. Wightman, E.C. Paik, S. Borman, A.M. Dayton, Anal. Chem. 50 (1978) 1410.
[6] B. Kastening, Anal. Chem. 224 (1967) 196.
[7] J.K. Dohrmann, F. Galluser, H. Wittchen, Faraday Discuss. Chem. Soc. 56 (1973) 350.
[8] R.D. Webster, R.A.W. Dryfe, J.C. Eklund, C.W. Lee, R.G. Compton, J. Electroanal. Chem. 402 (1996) 167.
[9] J. Wain, R.J. Compton, R. LeRoux, S.M. Matthews, K. Yunus, A.C. Fisher, J. Phys. Chem. B 110 (2006) 26040.
[10] J. Wain, R.J. Compton, R. LeRoux, S.M. Matthews, A.C. Fisher, Anal. Chem. 79 (2007) 1865.
[11] C. Fisher, K.A. Gooch, K. Yunus, D.W.E. Allsopp, T.J. Ryan, International Symposium of Chemical Characterization of Liquid/Liquid and Liquid/Membrane Interface for Development of Novel Reaction Fields, Kyoto, Japan, 2001.
[12] K. Yunus, C.B. Marks, A.C. Fisher, D.W.E. Allsop, T.J. Ryan, R.A.W. Dryfe, S. Hill, E.D. Roberts, Electrochem. Commun. 4 (2002) 579.
[13] S.S. Hill, R.A.W. Dryfe, E.P.L. Roberts, A.C. Fisher, K. Yunus, Anal. Chem. 75 (2003) 486.
[14] K. Yunus, I.E. Henley, A.C. Fisher, J. Phys. Chem. B 107 (2003) 3878.
[15] S.P. Sullivan, M.L. Johns, S.M. Matthews, A.C. Fisher, Electrochem. Commun. 7 (2005) 1323.
[16] I.E. Henley, A.C. Fisher, J. Phys. Chem. B 107 (2003) 6579.
[17] D. Horii, M. Atobe, T. Fuchigami, F. Marken, Electrochem. Commun. 7 (1) (2005) 35.
[18] S.K. Yoon, E.R. Choban, C. Kane, T. Tzedakis, P.J.A. Kenis, J. Am. Chem. Soc. 127 (2005) 10466.
[19] J. Krüger, K. Singh, A. O'Neill, C. Jackson, A. Morrison, P. O'Brien, J. Micromech. Microeng. 12 (2002) 486.
[20] A. Wolff, I.R. Perch-Nielsen, U.D. Larsen, P. Friis, G. Goranovic, C.R. Poulsen, J.P. Kutter, P. Telleman, Lab Chip 3 (2003) 22.
[21] A.Y. Fu, C. Spence, A. Scherer, F.H. Arnold, S.R. Quake, Nat. Biotechnol. 17 (1999) 1109.
[22] S.M. Matthews, A.D. Elder, K. Yunus, C.F. Kaminski, C.M. Brennan, A.C. Fisher, Anal. Chem. 79 (2007) 4101–4109.
[23] J.P. Jackel, Microtechnology 36 (1996) 707.
[24] G.M. Whitesides, E. Ostuni, S. Takayama, X. Jiang, D.E. Ingber, Annu. Rev. Biomed. Eng. 3 (2001) 335–373.